Type-II Clathrate $Na_{24-\delta}Ge_{136}$ from a Redox-Preparation Route

Xian-Juan Feng,[a] Matej Bobnar,[a, c] Swantje Lerch,[b] Harry Biller,[b] Marcus Schmidt,[a] Michael Baitinger,[a] Thomas Strassner,[b] Yuri Grin,[a] and Bodo Böhme*[a]

Abstract: The metastable type-II clathrate $Na_{24-\delta}Ge_{136}$ was obtained from $Na_{12}Ge_{17}$ by applying a two-step procedure. At first, $Na_{12}Ge_{17}$ was reacted at 70 °C with a solution of benzophenone in the ionic liquid (IL) 1,3-dibutyl-2-methylimidazolium-bis(trifluoromethylsulfonyl) azanide. The IL was inert towards $Na_{12}Ge_{17}$, but capable of dissolving the sodium salts formed in the redox reaction. By annealing at 340 °C under an argon atmosphere, the X-ray amorphous intermediate product was transformed to crystalline $Na_{24-\delta}Ge_{136}$ ($\delta \approx 2$) and α-Ge in an about 1:1 mass ratio. The product was characterized by X-ray powder diffraction, chemical analysis, and ^{23}Na solid-state NMR spectroscopy. Metallic properties of $Na_{24-\delta}Ge_{136}$ were revealed by a significant Knight shift of the ^{23}Na NMR signals and by a Pauli-paramagnetic contribution to the magnetic susceptibility. At room temperature, $Na_{24-\delta}Ge_{136}$ slowly ages, with a tendency to volume decrease and sodium loss.

Introduction

Since the discovery of the first binary intermetallic clathrates with homoatomic group-14 frameworks encaging alkali metals as guests in their polyhedral cages[1–3] (Figure 1), various types of this group of compounds have been described, ranging from complex multinary phases with guest or framework substitution[4–8] to guest-free metastable allotropes of silicon and germanium.[9–12] Intermetallic (anionic) clathrates feature positively charged guest and partially negatively charged framework atoms. The reverse host-guest polarity occurs in so-called inverse or cationic clathrates.[5] While ternary and higher multinary intermetallic clathrates have often been prepared directly from the elements by applying standard melt-based and solid-state techniques,[4–7] binary representatives typically require more elaborate techniques, of which high-pressure approaches have recently gained increasing attraction.[13] However, thermal decomposition of alkali-metal rich Zintl phases has been the original preparation method for binary alkali-metal clathrates.[1,2,14] After the early works, the influencing parameters for the thermal decomposition method have been further investigated,[15] and the technique has been further developed.[16,17] A thermal decomposition reaction may be realized as a redox process as exemplified by Equation (1), in which the superscript numbers represent the (average) oxidation numbers.

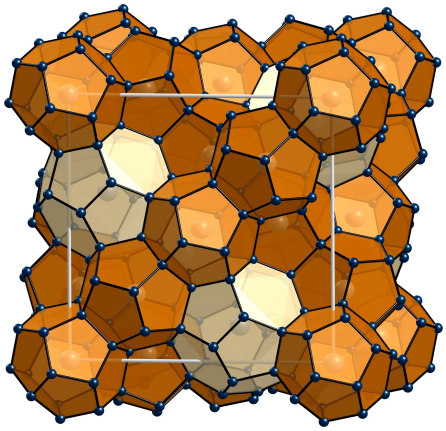

Figure 1. Type-II clathrate crystal structure of $Na_{24-\delta}Ge_{136}$ (space group $Fd\bar{3}m$) with the four-bonded Ge framework atoms represented as blue and the Na guest atoms as larger grey spheres. The pentagon-dodecahedral Ge_{20} cages (5^{12}) centered by Na1 atoms (site 16*c*) appear orange and the hexakaideca-hedral Ge_{28} cages ($5^{12}6^2$) centered by Na2 atoms (site 8*b*) appear yellowish. The bonds between the Ge framework atoms are drawn as black, unit-cell edges (origin choice 2) as white lines.

$$34\,Na^{(+1)}{}_4Ge^{(-1)}{}_4 \rightarrow 112\,Na^{(\pm 0)}{}_g + Na^{(+1)}{}_{24}[Ge^{(-24/136)}]_{136} \quad (1)$$

[a] Dr. X.-J. Feng, Dr. M. Bobnar, Dr. M. Schmidt, Dr. M. Baitinger, Prof. Y. Grin, Dr. B. Böhme
Max-Planck-Institut für Chemische Physik fester Stoffe
Abteilung Chemische Metallkunde
Nöthnitzer Straße 40, 01187 Dresden (Germany)
E-mail: bodo.boehme@cpfs.mpg.de

[b] S. Lerch, H. Biller, Prof. Dr. T. Strassner
Technische Universität Dresden
Fachrichtung Chemie und Lebensmittelchemie
Professur für Physikalische Organische Chemie
01062 Dresden (Germany)

[c] Dr. M. Bobnar
Jožef Stefan Institute
Jamova 39, 1000 Ljubljana (Slovenia)

Supporting information for this article is available on the WWW under https://doi.org/10.1002/chem.202102082

$$34\,Na^{(+1)}{}_4Ge^{(-1)}{}_4 + 112\,H^{(+1)}Cl^{(-1)} \rightarrow 112\,Na^{(+1)}Cl^{(-1)} + Na^{(+1)}{}_{24}[Ge_{136}{}^{(-24/136)}] + 56\,H^{(\pm0)}{}_2 \quad (2)$$

The driving force for a thermal decomposition reaction largely depends on the equilibrium vapor pressure of the respective metal over the precursor. Depending on the experimental setup and the transport conditions for the metal vapor, a minimum temperature is required for an effective conversion. Since these conditions do not always comply with the conditions suitable to conserve the target intermetallic clathrate phase, preparative approaches involving heterogeneous chemical redox processes by external oxidizers have been developed.[18–20] With that approach, a larger driving force is achieved due to the higher redox potential of oxidizers like HCl or alkyl chlorides, which mainly arises from the precipitation of metal halides and the evolution of stable gases like H_2 or alkanes (Eq. (2)). Provided that suitable reaction kinetics can be achieved in the solid state, these redox methods may thus be applied also at low temperature, where the formation of low-temperature phases is possible and metastable products may more likely be conserved. Only recently, the redox methods towards intermetallic clathrates have been further complemented by electrochemical approaches applying molten-salt[21] or solid-state electrolytes,[22] and also related electrochemically assisted methods using spark-plasma processes have been introduced.[23] Apart from the preparation of intermetallic clathrates, chemical and electrochemical redox methods have proven useful, particularly, for the closely related reaction pathways towards the initially-mentioned metastable clathrate-type allotropes,[9–12] consisting of the emptied clathrate frameworks, only. In similar ways, other crystalline metastable allotropes of Si and Ge[24] without a thermodynamic existence field in the *p-T* diagrams,[25] as well as nanostructured and surface-stabilized forms of group-14 elements have been obtained.[18,26–29]

An intermetallic clathrate phase, which was discovered already within the early works by Hagenmuller et al.,[2,30,31] is Na_xGe_{136}. Its preparation, particularly with large Na concentration, has remained a challenge ever since, however. The phase has originally been obtained by thermal decomposition of Na_4Ge_4 only as a minor by-product[30] besides α-Ge and Na_4Ge_{13},[32] and solely within a narrow temperature window around 360 °C.[30,33] Only recently, bulk quantities of the phase with low Na concentration ($x \approx 5$) have been obtained at $T \geq 300$ °C by using a modified thermal decomposition technique, which provides better control of the Na vapor pressure and transport, and seems to avoid the competing formation of Na_4Ge_{13}.[17] Also, thin-film preparation of Na_xGe_{136} ($0 < x < 24$) on α-Ge wafers by thermal decomposition has been reported only recently,[34] for which a distinctly lower temperature of only 300 °C was applicable, and a competitive formation of Na_4Ge_{13} did not occur. The established method for the preparation of Na_xGe_{136} ($x \rightarrow 0$) and the Ge(*cF*136) allotrope ($x = 0$) as bulk material has been the gas-solid oxidation of $Na_{12}Ge_{17}$.[19,35] On the other hand, this approach has not been suitable for the selective preparation of the phase with high sodium content $Na_{24-\delta}Ge_{136}$ (δ denoting a small deficiency), because an admixture also of the sodium-depleted phase Na_xGe_{136} ($x \rightarrow 0$) cannot be avoided.[36] The reduction of Ge(*cF*136) by alkali metal vapor, which was successful in the preparation of $K_{24-\delta}Ge_{136}$[35] or, starting from Na_xSi_{136}, for $Na_{24-\delta}Si_{136}$,[37] has not succeed in $Na_{24-\delta}Ge_{136}$ of good quality, either. Finally, the recently reported electrochemical approach, although providing potential for an improved reaction control with respect to $Na_{24-\delta}Ge_{136}$ and $Na_{x\rightarrow0}Ge_{136}$ still suffers from inevitable by-products tracing back to the applied electrolytes, and needs further optimization in that regard.[21]

Here we report on the selective two-step bulk preparation of the so far hardly accessible $Na_{24-\delta}Ge_{136}$, comprising the low-temperature oxidation of $Na_{12}Ge_{17}$ to an X-ray amorphous intermediate product as reported in detail in a preceding work,[38] which is converted to the final clathrate product by subsequent thermal treatment.

Results and Discussion

Preparation of $Na_{24-\delta}Ge_{136}$-Step 1

The first preparation step was the conversion of the starting material $Na_{12}Ge_{17}$ with benzophenone in the ionic liquid 1,3-dibutyl-2-methylimidazolium bis(trifluoromethyl-sulfonyl) azanide ([DBMIM][TFSI]) at 70 °C for 3 days.[38] The solid product **I** was obtained after separation from the liquid phase as dark-gray to black powder, which was widely X-ray amorphous (Figure 2). Only a tiny fraction of about 1 mass-% crystalline α-Ge was detected.[38] According to chemical analysis, the sodium content in product **I** was significantly lower than that of $Na_{12}Ge_{17}$, and a composition of about $NaGe_{6.25}$ was evaluated (Table 1). Assuming the initial formation of benzophenone radical anions,[38] the overall redox reaction of $Na_{12}Ge_{17}$ to product **I** with the given composition may be expressed by Equation (3).

$$Na_{12}Ge_{17} + 232/25\ (C_6H_5)_2CO \rightarrow 68/25\ NaGe_{6.25} + 232/25\ Na[(C_6H_5)_2CO^{\bullet}] \quad (3)$$

The content of elements expected for residues of the applied organic components in the reaction (C, H, O, N, S) was low. The small lack in the analytical total of product **I** might imply contributions of further elements. Actually, tantalum, silicon, aluminum, chlorine and oxygen were occasionally detected in spotty impurities adjacent to the main phase in SEM/EDX analyses (see Supporting Information, Figure S2). These impurities may originate from the ampoule used for the preparation of the $Na_{12}Ge_{17}$ starting material, from reactants or solvents used during the preparation of the IL and from the molecular sieve used to ensure the essential and steady absence of water in the IL on storage,[38] respectively.

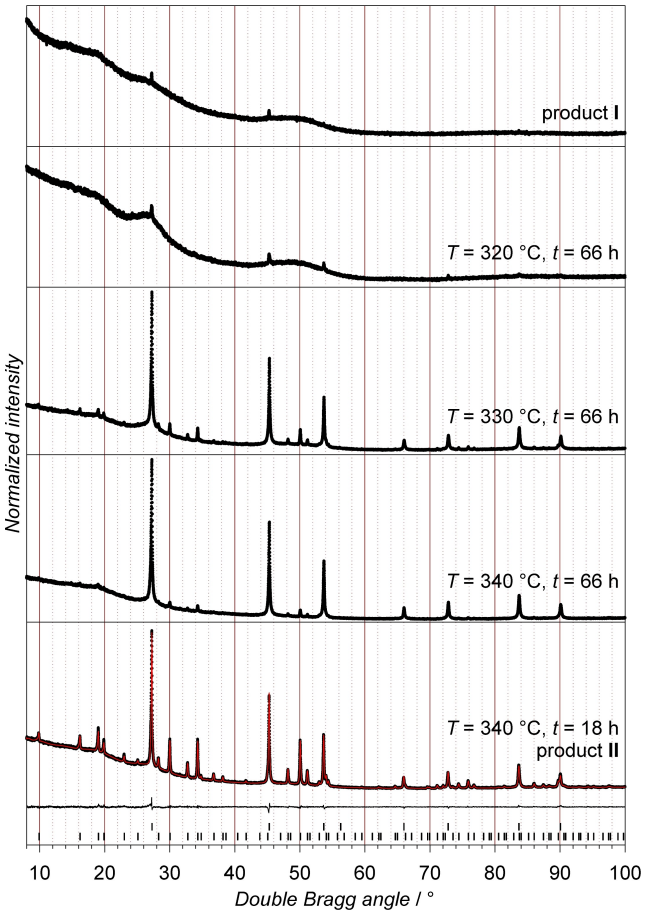

Figure 2. Preparation of $Na_{24-\delta}Ge_{136}$: XRPD patterns (Cu $K\alpha_1$) of product **I** and of the samples after its heat treatment at different conditions (black dots). For product **II**, also the calculated pattern obtained by Rietveld refinement (red line), the intensity residuals (black curve below) and the calculated reflection positions for α-Ge (upper tick row) and $Na_{22}Ge_{136}$ (bottom tick row) are plotted.

Preparation of $Na_{24-\delta}Ge_{136}$-Step 2

To elucidate the thermal and the crystallization behavior of product **I**, DTA-TG experiments followed by XRPD analyses of the used specimens were performed. Up to 700 °C, only a small mass-loss of less than 1% was observed, but several broad exothermic effects were detected (Figure 3). On measurements of several specimens at the same heating rate, but to different maximum temperature, these effects were qualitatively reproducible (Figure S5). While the two broad exothermic effects at 160 °C and 260 °C came along with discernable, likewise smeared, steps in the TG curve, the sharper effect at 410 °C and the two weaker effects at 460 °C and 510 °C did not show such a coincidence. Further distinct mass loss was observed only above 600 °C.

The XRPD investigations after the DTA-TG measurements showed that the exothermal effects below 300 °C should be associated to the crystallization of small amounts of $Na_{12}Ge_{17}$ and Na_4GeO_4. Besides the small amount of α-Ge already present in product **I**, both phases were identified by their strongest characteristic reflections in the specimen after the measurement to $T_{max} = 300$ °C (Figure 4). The stronger exothermic effect at 410 °C was found to be associated to the crystallization of α-Ge and $Na_{24-\delta}Ge_{136}$. After heating to $T_{max} = 430$ °C, both phases were detected in the respective specimen, besides a small contribution of Na_4GeO_4. $Na_{12}Ge_{17}$ was not detected, however. Finally, the exothermic signals at 460 °C and 510 °C were found to be associated to the decomposition of the clathrate phase at the applied heating rate, and also to a transformation of Na_4GeO_4 into Na_2GeO_3. After the measurement to $T_{max} = 700$ °C, the specimen contained mainly crystalline α-Ge, besides a small fraction of Na_2GeO_3 (Figure 4). Details of the mechanisms still have to be investigated, but evidently, an overall mass-loss of the specimen is neither involved with the formation nor with the decomposition of the clathrate phase and, as well, not with the transformation of the ortho-germanate. Moreover, $Na_{24-\delta}Ge_{136}$ is likely to decompose exothermally, so that its metastability may be concluded at the investigated conditions.

Since the exothermic effect at 410 °C was associated to the formation of crystalline $Na_{24-\delta}Ge_{136}$ and α-Ge on dynamic heating, another DTA-TG investigation to the lower $T_{max} =$ 350 °C, with a subsequent annealing time of 4 h at that temperature, was performed (Figure S5). As expected, α-Ge and $Na_{24-\delta}Ge_{136}$ were observed in the specimen by XRPD afterwards. Also a small contribution of Na_2GeO_3 was revealed (Figure 4). Annealing of product **I** at 350 °C should thus enable the preparation of $Na_{24-\delta}Ge_{136}$. However, the preparation of bulk

Table 1. Chemical composition of product **I** obtained by the redox-step in the IL and of product **II** obtained by subsequent thermal treatment at 340 °C for 18 h: Measured mass fractions (*w*) and the derived molar equivalents for the elements normalized to one sodium equivalent *N*(*E*). Calculated molar equivalent values for $Na_{12}Ge_{17}$ used as the starting material and for a hypothetical phase mixture of $Na_{22}Ge_{136}$ and α-Ge in a 45/55 mass-ratio are given for comparison.

	$Na_{12}Ge_{17}$	Product **I**		Product **II**		$Na_{22}Ge_{136}$ + α-Ge
Element	*N*(*E*)	*w*/%	*N*(*E*)	*w*/%	*N*(*E*)	*N*(*E*)
Na	1	4.67(6)	1.000(13)	4.73(8)	1.000(17)	1
Ge	1.42	92.1(12)	6.25(8)	92(2)	6.17(15)	14.12
O		0.88(2)	0.271(6)	0.89(1)	0.270(3)	
N		0.05(2)	0.018(8)	0.06(1)	0.021(3)	
C		0.386(5)	0.158(2)	0.252(5)	0.102(2)	
H		0.076(1)	0.371(5)	0.014(1)	0.068(5)	
S		0.193(1)	0.02963(15)	0.19(1)	0.0288(15)	
Total		98.4(12)		98(2)		

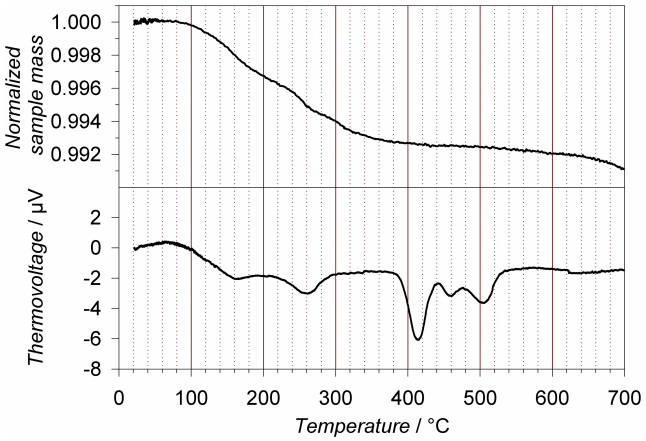

Figure 3. DTA-TG investigation of product **I** on heating at 10 K/min.

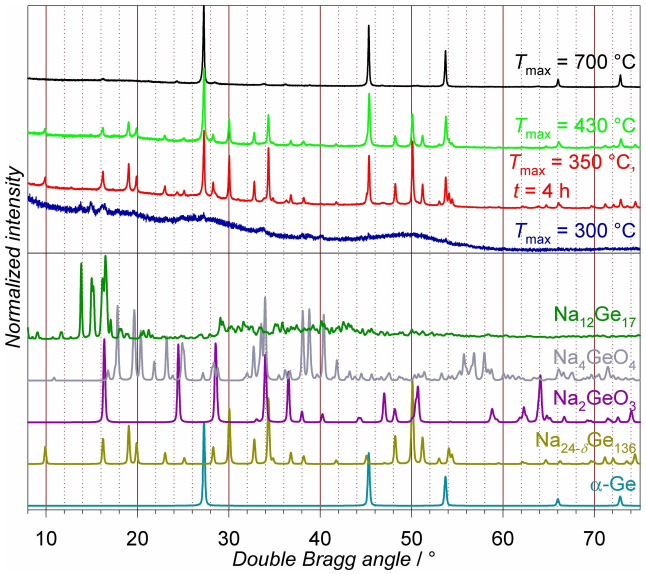

Figure 4. (top) Experimental XRPD patterns (Cu $K\alpha_1$) of the specimens after the DTA-TG measurements of product **I** to the given maximum temperature T_{max} and an optional annealing for a time t (the color code corresponds to the one in Figures 3 and S5); (bottom) Calculated XRPD patterns for α-Ge,[39] the type-II clathrate phase $Na_{24-\delta}Ge_{136}$,[2] Na_2GeO_3,[40] Na_4GeO_4[41] and $Na_{12}Ge_{17}$.[42]

samples at 350 °C was found challenging. By principle, the temperature control on larger samples and by using a tube furnace is less precise than in a thermobalance. With only a short reaction time needed at 350 °C, the crystallinity and the composition of the product were, therefore, hardly reproducible. On the other hand, a too low temperature of $T = 320$ °C did not lead to a crystalline product, even after prolonged annealing for 66 h. By XRPD, only a small amount of α-Ge, similar to the already present one in product **I**, was observed. Oxides or $Na_{12}Ge_{17}$ were not revealed in the specimen, however (Figure 2). The changes in the measured background already hinted on some structural reorganization on the nanometer scale. After heat treatment for 66 h, but at $T = 330$ °C, the presence of crystalline $Na_{24-\delta}Ge_{136}$ and α-Ge was confirmed (Figure 2). But, a large contribution of α-Ge and only a small fraction of crystalline $Na_{24-\delta}Ge_{136}$ were found, while about half of the sample still was X-ray amorphous. A further increase of the annealing temperature to 340 °C, and annealing for likewise 66 h, resulted in a widely crystalline product. Nevertheless, only a similarly small fraction of $Na_{24-\delta}Ge_{136}$ was found (Figure 2). The product thus consisted mainly of crystalline α-Ge. Comprehensibly, a too long annealing time may lead to a widely crystalline product, but to proceeding decomposition and thus to lower yield of the metastable $Na_{24-\delta}Ge_{136}$ phase. When the annealing time was shortened to 18 h while keeping the annealing temperature at 340 °C, the content of crystalline $Na_{24-\delta}Ge_{136}$ distinctly increased. At these conditions, the clathrate phase was reproducibly found in an about 1:1 mass-ratio with α-Ge, while only a small fraction of the sample (typically below 10 mass-%, see below) remained undetected by XRPD. For a selective preparation of the clathrate phase, an annealing temperature of 340 °C and an annealing time of about 18 h is thus considered most favorable. The XRPD pattern of a typical product obtained by this annealing procedure is shown in Figure 2. This sample was extensively characterized and will be referred to as product **II** in the following.

Crystal structure of $Na_{24-\delta}Ge_{136}$ and sample composition of product II based on XRPD

$Na_{24-\delta}Ge_{136}$ crystallizes in the space group $Fd\bar{3}m$ (no. 227). The structure solution[43,44] from the XRPD data (Figure 2) exactly matched the original structure model for a type-II clathrate[2] (Table 2). This makes an appropriate description with the Na atoms localized in the cage centers, i.e. on Wyckoff sites 16*c* and, particularly, on 8*b* probable, the latter of which had been questioned for the related type-II clathrate $Na_{24}Si_{136}$.[23] Initially, the structure refinement by the Rietveld method included the scale factor, the lattice parameter, the positional parameters of Ge2 and Ge3, the isotropic thermal displacement parameters (U_{iso}) for all sites, as well as the phase fraction, the lattice parameter and the displacement parameter of the Ge1 atom for the second phase α-Ge. The refined positional parameters yielded expectable interatomic distances for the Ge framework (Tables S1 and S2). The displacement parameters of the framework atoms had equal values within the estimated standard deviation, and approached the one refined for α-Ge. This result indicated a reasonable scale factor as well as meaningful phase fractions of 45 mass-% for the clathrate phase and 55 mass-% for α-Ge. On the other hand, the displacement parameter of Na2 was peculiarly large (U_{iso}(Na2) > 0.2 Å^2). As an off-center split atomic position for Na2 in the large Ge_{28} cages could not be revealed, the result suggested a reduced occupancy. Due to the low scattering power of Na as compared to Ge and the limitations by the XRPD data, a correlation of the occupancy factor for Na2 with the displacement parameters occurred, and a lowered, but inappropriately uncertain U_{iso}(Na2) was obtained (Table S1). Finally, two refinements were performed, for which either the displacement parameter or the occupancy factor of the Na2 site were fixed and incrementally altered, while the

Table 2. Crystallographic data of $Na_{22}Ge_{136}$ and α-Ge (both space group $Fd\bar{3}m$, OC 2) obtained by Rietveld refinement of XRPD data of product **II**.

Atom label	Wyckoff site (coordinates)	Refined parameters		$Na_{21.4(7)}Ge_{136}$[a]	α-Ge
Na1	16*c* (0 0 0)	*occ*		1*	
		U_{iso}/Å^2		0.022(16)	
Na2	8*b* (3/8 3/8 3/8)	*occ*		0.67(9)	
		U_{iso}/Å^2		0.125*	
Ge1	8*a* (1/8 1/8 1/8)	U_{iso}/Å^2		0.016(6)	0.0131(11)
Ge2	32*e* (*x x x*)	*x*		0.2182(4)	
		U_{iso}/Å^2		0.013(4)	
Ge3	96*g* (*x x z*)	*x*		0.0674(2)	
		z		0.3715(4)	
		U_{iso}/Å^2		0.010(3)	
		mass fraction	- relative	0.442(8)	0.558(8)
			- absolute[b]	0.42	0.51
		a/Å	- Rietveld	15.4408(12)	5.6575(4)
			- vs. LaB_6[c]	15.4355(4)	5.6551(2)
applied Bérar factor[d]				5.2	
R_P[e]				0.015	
R_B(obs)[e]				0.042	0.056

[a] Parameters fixed during the last refinement cycle are marked with an asterisk. [b] Typical value deduced from Rietveld refinement on XRPD data from specimens with admixed LaB_6 intensity standard. [c] The lattice parameters were calculated vs. LaB_6 internal standard by using an XRPD dataset obtained in a separate measurement, which was performed with a time delay of about 2 h after the measurement used for structure refinement. [d] The Bérar factor is the ratio *S*′/*S* of estimated standard deviations (e.s.d.) calculated by the Bérar method (*S*′)[47] and of e.s.d. conventionally calculated by treating the errors of the profile fit for individual data points as purely statistical (*S*).[43] [e] R_P is the residual value for the profile fit with y_i denoting point intensity: $R_P = \Sigma_i |y_{i,obs} - y_{i,calc}| / \Sigma_i |y_{i,obs}|$; R_B(obs) is the residual value for integrated intensities I_j of the Bragg reflections classified as observed after background subtraction: $R_B(obs) = \Sigma_j |I_{j,obs} - I_{j,calc}| / \Sigma_j |I_{j,obs}|$.[48]

respective other one was refined together with all other parameters. The final result was each indicated by the same minimum in the Bragg residual value R_B (Table S1). For both restrained refinements, the obtained *occ*(Na2) and U_{iso}(Na2) approached the same values within the estimated standard deviation (e.s.d). The finally revealed displacement parameter of Na2, furthermore, had a similarly large value as it had been observed for the related $Na_{24}Si_{136}$, if described with the same type-II clathrate structure model with non-split Na2 position.[23] Concerning the Na1 site, the occupancy factor slightly decreased on unfixing, but remained 1 within three times the e.s.d. Moreover, the displacement parameter got negative on reduced occupancy of Na1, hinting on a mismatch of actually observed and assigned electron density due to correlating parameters. In conclusion, the Na1 site was considered fully occupied by Na, and its occupancy factor was fixed to 1 for the final refinement cycle (Tables 2, S1). The calculated or assigned phase compositions from the refinement results, $Na_{21.4(7)}Ge_{136}$ and $Na_{22.14}Ge_{136}$, were practically equal within one e.s.d., so that the clathrate composition in product **II** is considered to be about $Na_{22}Ge_{136}$. This composition actually is consistent with the observed lattice parameter of $a = 15.4355(4)$ Å, which is somewhat smaller than 15.4412(7) Å of the recently reported slightly sodium-richer composition $Na_{23.0(5)}Ge_{136}$.[21] However, while the difference in the lattice parameter between both clathrate products is significant, the composition difference is actually close to the resolution limit on basis of the XRPD data used in both cases. By using LaB_6 as an internal standard for reflection intensities in Rietveld refinement, $Na_{22}Ge_{136}$ and α-Ge were found to actually represent almost the entire mass of the sample (Table 2). Product **II** was thus almost completely crystalline, and only a small mass-fraction of the sample (5 to 10 mass-%) was not detected by XRPD. By investigating several specimens of product **II** with LaB_6 standard in that way, the 45:55 relative mass ratio of $Na_{22}Ge_{136}$ and α-Ge as well as the concluded mass fraction of not detected phases remained unchanged. Only in one exceptional case, about 25 mass-% of the specimen was estimated not to contribute to Bragg diffraction, showing that product **II** may feature inhomogeneities with respect to the degree of crystallinity. Also, small reflections hardly rising above the background, were occasionally observed in the XRPD patterns of the product **II** specimens, hinting on traces of crystalline impurities. However, differently to the specimens investigated after DTA-TG measurements, an unambiguous assignment in product **II** was not possible due to the very low intensity of the reflections.

Transient character of $Na_{24-\delta}Ge_{136}$ at room temperature

$Na_{24-\delta}Ge_{136}$ in product **II** was found to be subject to distinct changes at room temperature on time scales of hours to months. The aging on air and in argon atmosphere was traced by XRPD (Figure 5). Although the changes were found slower on storage in argon atmosphere, the principle behavior remained the same as on storage in air (Figure 6). A degradation solely due to reaction with moisture or oxygen may thus be excluded. Moreover, also a temperature increase to 70 °C additionally investigated in argon atmosphere led to acceleration of the changes, which further evidences the solely kinetic stability of the phase, and the low activation barrier for the observed aging process. The eye-catching changes of the clathrate phase on aging were a decrease of the lattice parameter (Figure 6), coming along with distinct, angle-dependent broadening of the Bragg reflections (Figure 5, Figure S1).

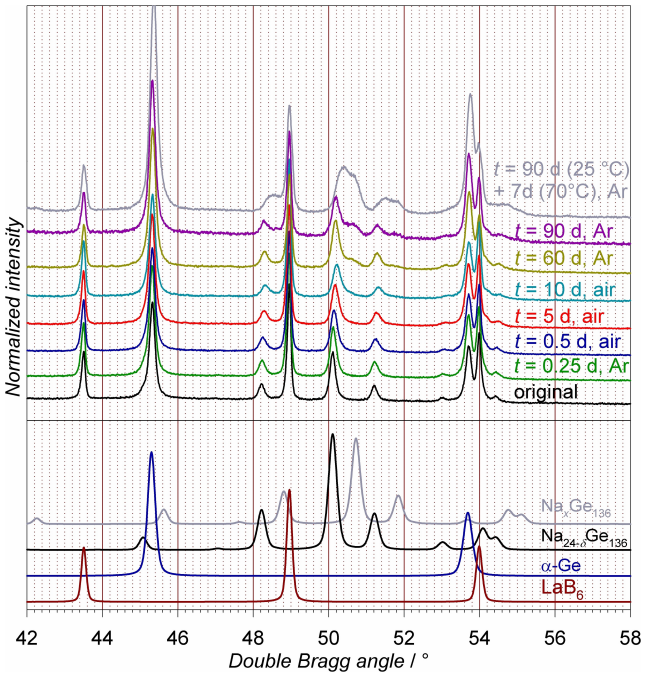

Figure 5. (top) Selected region of X-ray diffraction patterns of product **II** measured after storage on air or in an argon glovebox for the given times. If not otherwise mentioned, the specimens were stored at room temperature for the whole time. (bottom) Calculated XRPD patterns for LaB_6,[49] α-Ge[39] and a type-II clathrate phase[2] at sodium-rich composition $Na_{22}Ge_{136}$ ($a = 15.4355$ Å) and Na_xGe_{136} ($x \rightarrow 0$, $a = 15.26$ Å).

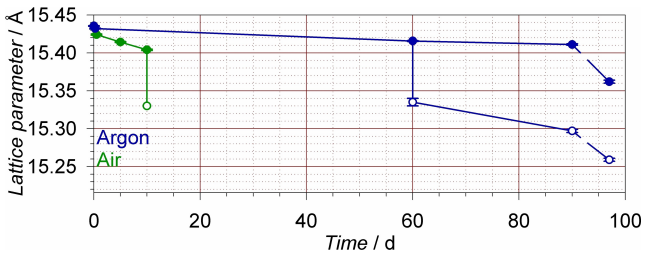

Figure 6. Development of the lattice parameter of $Na_{24-\delta}Ge_{136}$ on aging in air or argon atmosphere. Open symbols represent the values for the sodium-deficient phase Na_xGe_{136} forming after longer time periods. The dataset for 97 days was obtained from the sample stored in argon for 90 days and subsequently annealed at 70 °C for another 7 days.

Moreover, after longer storage time, a second isotypic clathrate phase with distinctly smaller lattice parameter formed.

According to Williamson-Hall analysis,[43,45] the reflection broadening is assigned to increasing strain in the particles rather than to a decreasing size of coherently scattering domains (Figure S1). Only the segregated second clathrate phase with distinctly smaller lattice parameter also featured a further contribution to reflection breadth likely stemming from smaller scattering domain size. Further annealing at 70 °C seemed to come along with a release of strain as well as with a growth of the scattering domains for the phase with smaller lattice parameter.

In comparison to the original product **II** before aging, the structure refinement of the clathrate phase was further challenged by the reflection broadening, particularly in the presence of a second isotypic clathrate phase. The increasingly problematic intensity deconvolution of reflections and background, particularly of the strongly broadened high-angle reflections, may lead to biased thermal displacement parameters and also affect the refined positional parameters. Moreover, a not straightforward deconvolution of the severely overlapped low-angle reflections of the two isotypic clathrate phases complicated the refinement of the phase composition (Tables S3 and S4).

For the aging series on air, significant changes in the positional parameters of $Na_{24-\delta}Ge_{136}$ were not observed (Table S3). Changes of the clathrate composition could not be revealed. As well, the assigned phase fractions including the LaB_6 standard were constant within the estimated standard deviation of the refinement, even when the second type-II clathrate phase with smaller lattice parameter had formed with small mass content after 10 days. Therefore, there was no hint on a growing contribution of X-ray amorphous phase and on a decomposition of the clathrate phase as such. The prominent difference observed for $Na_{24-\delta}Ge_{136}$ in comparison to the refinement before aging (Table 2) was an increased thermal displacement parameter for the Ge1 and Ge2 atoms. These two Ge sites define perfectly tetrahedral structural entities by geometric restriction, centering super-tetrahedral units of the dodecahedral cages.[2,46] With a lack of positional degrees of freedom to adapt to disorder in the surrounding, the observation may indicate a decreasing Na occupancy of the dodecahedral cages, which, however, was not resolvable based on the Na1 occupancy factor. Increasing strain as observed from the reflection broadening (Figure S1) is an expectable consequence. A similarly strong influence of the Na2 occupancy seems unlikely, because in the product **II** material before aging, Ge1 and Ge2 show regular displacement parameters despite of an already deficient Na2 site. In the samples after longer storage in argon atmosphere, again, significant changes in the crystallographic parameters besides the lattice parameter were not revealed for the clathrate phase with larger lattice parameter. Only after further annealing at 70 °C for 7 days, the Na1 occupancy was found somewhat reduced (Table S4). For the second clathrate phase with distinctly smaller lattice parameter, both the dodecahedral and the hexakaidecahedral cages were found with low Na occupancy. With the challenges in the reflection profiles and the severe overlap of low-angle reflections, a more precise determination of the Na occupancy factors was not possible, however.

Chemical analysis of product II

According to chemical analyses, product **II** and its X-ray-amorphous precursor material product **I** before thermal treatment had practically the same composition (Table 1). A significant difference was detected only for the C and H impurities, which hints on a loss of organic residues during the

annealing process. The sum of the C and H mass loss of about 0.2% agrees in magnitude with the mass loss of about 0.5% recognized after annealing and is, likewise, qualitatively and quantitatively in line with the results of the DTA-TG investigations. The slight deviation might originate from an additional loss of elements such as Al, Si or Cl (Figures S2 and S3) not considered in chemical analysis. The molar ratio of Na and Ge was not affected by the thermal treatment, so that the crystallization of $Na_{24-\delta}Ge_{136}$ and α-Ge is clearly not a result of a thermal degradation coming along with an evaporation of sodium.[2,33] This conclusion is also corroborated by the unchanged morphology of the powder particles and agglomerates in product **I** and product **II** revealed by SEM (Figures S2 and S3). Moreover, it agrees with the results of the DTA-TG investigations, where crystallization of α-Ge and $Na_{24-\delta}Ge_{136}$ was not accompanied by a mass loss either.

The molar ratio of Na and Ge (10:62 ≈ 22:136) revealed for the bulk of product **II** by chemical analysis was close to that of the type-II clathrate phase contained in it. On the other hand, a much lower Na content was expected for a mixture of $Na_{22}Ge_{136}$ and α-Ge at the mass ratio of 45:55 from Rietveld refinement (Table 2). Product **II** is thus found much richer in Na by chemical analysis than expected on basis of the crystalline phases. An error of chemical analysis is unlikely because the composition of product **II** agrees with that of product **I**, and a noticeable mass-loss has not been observed, as discussed above. Also EDXS analyses on the powder specimen investigated in SEM (Figure S3) revealed a Na:Ge molar ratio of about 1:7 on average, while hinting on local variance of the ratio and thus suggesting the presence of more than one phase. The Na:Ge ratio supports the result of chemical analysis, if considering the powder state of the specimen and a partial overlap of the analyzed Na *Kα* with the dominant Ge *Lα* line, hampering more precise analysis.

In XRPD, α-Ge had sharp and symmetric reflections (Figure 5), and the lattice parameter of $a = 6.5551(2)$ Å (Table 2) determined against LaB_6 internal standard was close to that reported for pure α-Ge ($a = 5.65748(4)$ Å[39]). Na as a part of the crystal structure of α-Ge in relevant concentration may thus be excluded as an explanation for the large Na content of product **II**. This seems unlikely anyway, as a large solubility of Na in diamond-type α-Ge has never been reported. As well, from Rietveld refinement there was no indication for a Na occupancy in the cages of the type-II clathrate larger than the ideal $Na_{24}Ge_{136}$. So far, such a case has been reported only for the related $Na_{24+\delta}Si_{136}$ obtained at high-pressure conditions.[13f] Framework substitution of the type-II clathrate by Na atoms similar to other alkali-metal clathrates like the Li-containing $Na_{16}Cs_8Li_xGe_{136-x}$[46] or the framework-substituted type-III clathrate $Cs_{30}(Na, Sn)_{172}$[50] may be excluded as well, particularly, if considering the large Na content required in such a case to reasonably explain the result of chemical analysis. Therefore, it is evident that the small mass fraction of product **II** not detected by XRPD (Table 2) contains a large portion of the total Na content of the sample.

As the presence of the germanates Na_2GeO_3 and Na_4GeO_4 was observed in the specimens after DTA-TG investigations, it seems straightforward to assume the presence of such a kind of oxidic by-products also for the bulk-sample of product **II**. However, to comprise half or even more of the sodium content of the sample, a mass content of the by-product of at least 6% was required, if Na_4GeO_4, featuring the largest relative sodium content, was assumed. This is inconsistent with the low and not assignable amount of crystalline by-products detected in product **II** by XRPD. Moreover, a larger oxygen content was required than actually detected by the chemical analysis, which would allow for at most 3.2 mass-% of Na_4GeO_4 in the sample. Therefore, also other sodium-containing phases such as $Na_{12}Ge_{17}$, possibly of low crystallinity, should be present on the order of 5 to 8 mass-%. The consequent conclusion of sodium-containing by-products with a total mass-fraction of about 10% is in good agreement with the content of phases not assigned or observed in the XRPD patterns. As well, the presence of germanates and germanides may reasonably explain the distinctly basic reaction of product **II** on contact with water.

^{23}Na solid-state NMR spectroscopy

As expected for a sample containing a type-II clathrate phase with almost completely Na-filled cages,[51,52] the ^{23}Na spectra of product **II** revealed two distinctly downfield-shifted signals. Together with the short relaxation times, which were estimated to be in the range of only 100 ms, this hints on strong Knight shifts due to conduction electrons. The signals are denoted with a_1 and a_2 in the static spectrum (Figure 7). Additionally, a third, in comparison to a_1 and a_2, much sharper and slightly asymmetric signal a_3 was observed in the static spectrum, which is assigned to non-metallic secondary phases and will be discussed later in more detail.

The symmetric signal a_1 with an isotropic shift of about 1200 ppm showed strong quadrupole coupling with a coupling constant of 308 kHz, as extracted from a signal fit. In agreement with that, the respective signal obtained at MAS conditions featured rotational side bands, which were visible as broad humps particularly towards larger shift (Figure 7b). Signal a_1 therefore is assigned to Na1 atoms at site 16*c* (*Fd*$\bar{3}$*m*) centering the dodecahedral cages (Figure 1) with .$\bar{3}$*m* trigonal point symmetry, for which quadrupole coupling may be expected. The broadened and more asymmetric signal a_2 with an isotropic shift of about 1500 ppm thus should arise from Na2 atoms in the hexakaidecahedral cages. The lack of quadrupole coupling for that signal is in line with the $\bar{4}$3*m* cubic point symmetry of site 8*b* in the cage center. However, as the signal is broad and asymmetric, contributions of slightly different local environments are probable. Both a reduced occupancy of the Na2 site, but also partial off-center positions of Na2 atoms in the cages may be responsible. Weak characteristics of quadrupole coupling resulting from a corresponding non-cubic local symmetry for a part of the Na2 atoms might be unresolved.

For the integrated intensity ratio of the clathrate signals, a value of $I(a_1):I(a_2) \approx 2:1$ was observed (Table 3), which would actually be expected for a clathrate of ideal composition $Na_{24}Ge_{136}$. Considering that the intensities extracted from a fit of

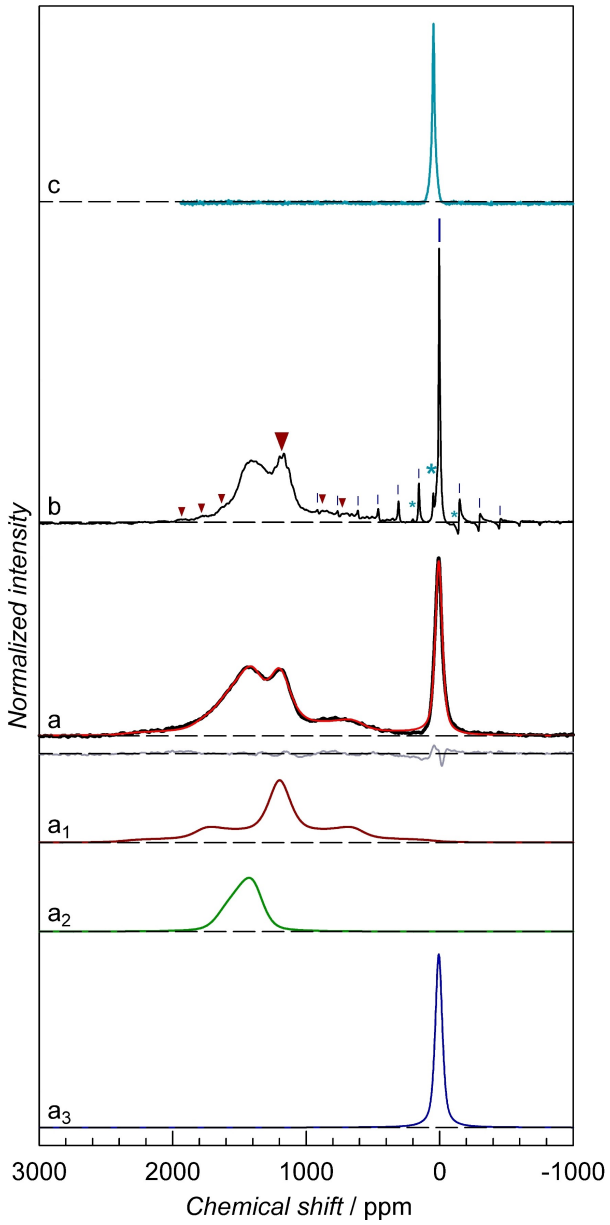

Figure 7. ^{23}Na NMR spectroscopy. (a) Spectrum of product **II** measured at static conditions (black curve) with a fit (red curve) considering the three individual signals a_1, a_2 and a_3 and leaving the residuals (grey curve) shown below. (b) Spectrum of product **II** measured at MAS conditions with a rotation frequency of 20 kHz revealing two signals close to 0 ppm, for which the central transitions and the rotational sidebands are marked with larger and smaller tick lines or asterisks, respectively. The comparably broad central transition and rotational side bands of signal a_1 are marked by red triangles. (c) Spectrum of $Na_{12}Ge_{17}$ measured at static conditions as a reference. Dashed horizontal lines represent zero intensity for each graph.

severely overlapping signals may feature larger uncertainty, this value is in fair agreement with the ratio of 2.6:1 expected for $Na_{22}Ge_{136}$, anyway. A particular problem arises from the non-perfect description of the satellite transitions of signal a_1, which were found broader than expected based on the central transition. In the fit, the intensity of signal a_1 may thus be underestimated, while, due to signal overlap, a part of the not suitably ascribed intensity is wrongly assigned to signal a_2. In

Table 3. ^{23}Na NMR spectroscopy of product **II** at static conditions (Figure 7a): Isotropic shift δ, relative integrated intensity I_{rel} and signal assignment.

Signal	δ/ppm	I_{rel}	Assignment
a_1	1200	0.504	Na1 (16*c*)
a_2	1500	0.273	Na2 (8*b*)
a_3	0(+47[a])	0.223	Na in non-metallic impurities

[a] The evaluation and assignment included the spectrum obtained at MAS conditions and the reference spectrum of $Na_{12}Ge_{17}$ (Figures 7b and 7c).

such a way, an intensity fraction of only 7.5% stemming actually from signal a_1 and wrongly assigned to signal a_2 may falsify the ratio from 2.6:1 to 2.4:1.2 = 2:1. An effect of non-suitable recording conditions on the intensity ratio of the signals was ruled out by pulse optimization. Moreover, there are several further features in the NMR spectrum besides the intensity ratio, which support the structure model of $Na_{22}Ge_{136}$ (Table 2): Concerning signal a_1, the symmetric signal shape and the small half-width of the central transition, which resembles the one of the Na signal in $Na_{16}Cs_8Ge_{136}$,[46] indicates a widely ordered environment for the sodium atoms at site Na1, supporting full Na-filling of the small cages. However, the stronger broadening of the satellite transitions, which, in contrast to the central transition, are sensitive not only to magnetic interactions but also to small variance in the electric field gradient, indicates disorder in the further surrounding. With the asymmetric and markedly broadened signal a_2 assigned to Na2, this disorder should be localized at Na2 and is explained by the presence of vacancies deduced from the structure refinement.

These conclusions are well in line with the relevant distance and coordination numbers of *d*(Na1-6×Na1) = 5.46 Å, *d*(Na2-12×Na1) = 6.40 Å and *d*(Na2-4×Na2) = 6.68 Å. A comparison shows that the *d*(Na1-Na2) is distinctly longer than *d*(Na1-Na1), at equal coordination number of 6, so that a vacancy at site Na2 may have minor influence on the local environment relevant for the signal of Na1. However, with similar *d*(Na1-Na2) and *d*(Na2-Na2), and a tetrahedral coordination of Na2 by other Na2 atoms, a vacancy at a Na2 position should strongly influence a probed neighboring sodium atom at site Na2, even in a homogeneous field of 12Na1 atoms. To conclude, the structure model of $Na_{22}Ge_{136}$ showing a reduced sodium occupancy at site Na2 (8*b*) agrees with the characteristics and also with the integrated intensity ratio for the signals a_1 and a_2.

Besides the structure model for $Na_{22}Ge_{136}$, also the sample composition deduced from XRPD and chemical analysis is widely supported by the NMR spectrum of product **II**. Actually, the third signal a_3 at close to 0 ppm indicates the presence of a considerable fraction of cationic Na^+ species in the sample. Even more, the slightly asymmetric signal a_3 at static conditions (Figure 7a) was revealed to actually comprise the contributions of, at least, two chemically different Na species by the spectrum obtained at MAS conditions (Figure 7b). The larger signal component at a shift of 0 ppm was assigned to salt-like components in product **II**. Among them might be compounds such as sodium germanates, the presence of which has been

indicated by XRPD after DTA-TG investigation and chemical analysis of product **II**. The smaller contribution to signal a_3, having an isotropic shift of 47 ppm as revealed from the respective signal at MAS conditions, might originate from $Na_{12}Ge_{17}$ or a related cluster compound, the presence of which seems plausible with the above investigations as well. The reference spectrum measured for $Na_{12}Ge_{17}$ showed a relatively sharp and symmetric signal at the identical isotropic shift (Figure 6c). The shift was found close to the one observed for sodium atoms in the chemically related compound Na_4Si_4.[52] Although $Na_{12}Ge_{17}$ has a complex crystal structure, the pseudo-hexagonal arrangement of the cluster entities and sodium atoms[42] seems to provide similar coordination environments for all crystallographically different sodium atoms, so that their ^{23}Na NMR signals actually merge to the observed sharp total signal.

The relative quantification of Na contained in the clathrate phase and that in the non-metallic by-products of product **II** based on ^{23}Na NMR was complicated by the different relaxation times and the large differences in the resonance frequencies of the different species. As pulse frequency, pulse length, and the delay times were optimized for the clathrate signals a_1 and a_2, the a_3 signals of the by-products in the depicted spectra (Figure 7) actually appeared with reduced intensity. Also, the visible phase mismatch for the signals close to 0 ppm in the MAS spectrum (Figure 7b) stems from the non-ideal recording conditions for these signals. A pulse optimization series revealed that the absolute intensity for signal a_3 in the spectrum at static conditions (Figure 7a) actually represents less than 50% of the absolute intensity at optimal conditions for this signal. Therefore, the integrated signal intensity ratio of Na atoms of the clathrate phase to those of the by-products $I(a_1+a_2)/I(a_3) = 78/22$ extracted from the signal fit (Figure 7a, Table 3) actually translates into a molar ratio of Na atoms in the clathrate phase to Na atoms in the by-products approaching 1:1. The results of ^{23}Na NMR thus also support the conclusion, that about half of the Na content found for product **II** by chemical analysis actually was contained in by-products, which were not assigned as crystalline phases in XRPD. The overall composition of product **II** is thus also reasonably reflected in the ^{23}Na solid state NMR spectra. Only the relative amount of Na in $Na_{12}Ge_{17}$ or other cluster compounds and the signal at 0 ppm seems to disagree. However, as $Na_{12}Ge_{17}$ is very sensitive to moisture and air and the NMR experiments could not be performed in a totally inert environment, a part of sensitive germanides like $Na_{12}Ge_{17}$ might have reacted already to salt-like products such as NaOH or sodium germanates during the initial recording of the static spectrum and, possibly at a higher rate, on MAS conditions, which may lead to a slight temperature increase of the specimen.

Magnetic susceptibility of product II

A specimen of product **II** investigated 4 weeks after preparation featured diamagnetic behavior (Figure 8). Only towards low temperature, the magnetic susceptibility extrapolated to infinite external field revealed weak temperature dependence by a distinct upturn, which indicates the presence of weak Curie paramagnetic contributions. Those may arise from point defects, trace back to small paramagnetic impurities in the sample or to localization of electrons to sodium atoms in the cages.[2] The temperature-independent contribution to the specific magnetic susceptibility was extracted by using a fit according to Equation (4) for the data $T \geq 80$ K.

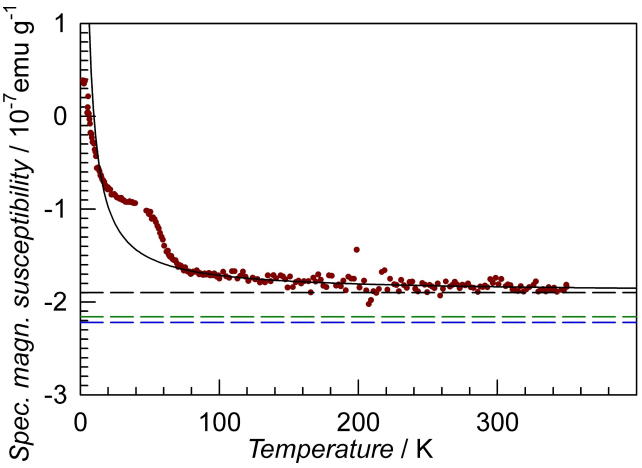

Figure 8. Specific magnetic susceptibility of product **II** extrapolated to infinite external field vs. absolute temperature (red dots). The hump at $T \approx 40$ K likely originates from residual oxygen in the measuring system. A fit according to Equation (4) for data $T \geq 80$ K (solid black line) yielded the temperature-independent term $\chi_{s,0}$ (dashed black line); the sum of diamagnetic increments calculated for the sample composition as obtained by chemical analysis (blue dashed line, Table 1) or for an assumed phase mixture of 45 mass-% $Na_{22}Ge_{136}$ and 55 mass-% α-Ge (green dashed line) are plotted for comparison.

$$\chi_s(T) = c/T + \chi_{0rs} \quad (4)$$

The observed value of $\chi_{0rs} = -1.90 \times 10^{-7}$ emu g^{-1} indicates a weaker diamagnetism than expected from the sum of the diamagnetic increments calculated for a sample composition of 45 mass-% $Na_{22}Ge_{136}$ and 55 mass-% α-Ge by using the molar increments for Na^+[53] and elemental four-bonded Ge^0 in α-Ge[54] (Figure 8). If also the contribution of the impurities is accounted for by using the nominal sample composition from chemical analysis (Table 1) and, as an approximation, besides the above increments for Na^+ and (4b)Ge^0 thus also the ones for O^{2-}, C^{4+}, N^{5+}, S^{4+}[53] are considered, a somewhat larger deviation is estimated (Figure 8). Irrespective of such uncertainty, by using the diamagnetic increment value for α-Ge, the increment of (4b)Ge^0 in the clathrate should, by principle, be underestimated in its absolute value due to the larger mean atomic volume of a germanium atom in the clathrate framework and other structural contributions coming along with a non-ideal tetrahedral environment for most of the germanium atoms in the clathrate as similarly discussed before[2] and also revealed for amorphous Ge.[54] Hence, the expected diamagnetism should lead to an even more negative temperature-independent susceptibility contribution than estimated from

the above sums of increments, so that a distinct positive deviation of the actually observed diamagnetism of the sample from the expected value is evident, and a temperature-independent Pauli-paramagnetic contribution is conclusive. $Na_{22}Ge_{136}$ is thus revealed to be a metal-like conductor. This result is well in line with the Knight shifts observed for the clathrate signals in ^{23}Na NMR and with the behavior expected for such a metal-rich composition of an intermetallic type-II clathrate.[2,55]

Conclusion

The oxidation of $Na_{12}Ge_{17}$ by benzophenone in the ionic liquid 1,3-dibutyl-2-methylimidazolium bis(trifluoromethyl-sulfonyl) azanide at 70 °C for 3 days leads to a widely X-ray amorphous product, which is thermally converted at 340 °C for 18 h to a crystalline product containing $Na_{24-\delta}Ge_{136}$ ($\delta \approx 2$) and α-Ge typically in a 45:55 mass ratio. The crystallization comes along practically without changes in the overall sample composition and without a mass loss, so that a reorganization in solid-state is evident. X-ray amorphous or not detectable crystalline by-products in the range of 10 mass-% gather a significant part of the nominal sodium content, which explains the apparent contradiction between the sample composition from chemical analysis and the one deduced from Rietveld refinement of X-ray powder diffraction data. The result is corroborated by the kind and quantity of sodium-containing by-products revealed by ^{23}Na NMR. $Na_{24-\delta}Ge_{136}$ ($\delta \approx 2$) is diamagnetic and shows metallic behavior as evidenced by Knight-shifted ^{23}Na signals in agreement with a Pauli-paramagnetic contribution to the magnetic susceptibility. At room temperature $Na_{24-\delta}Ge_{136}$ ($\delta \approx 2$) is metastable, showing, in both air and argon atmosphere, a complex transformation behavior on time scales of hours to months: Initially, the lattice parameter decreases, which comes along with XRPD detectable strain in the scattering domains and structural peculiarities suggesting reorganization, but not with resolvable changes of the overall clathrate composition. After longer time, a sodium-poor type-II clathrate with distinctly smaller lattice parameter segregates, and an overall sodium-loss from the clathrate phases becomes evident. The process is significantly accelerated at only slightly enhanced temperature (70 °C), conclusively indicating a low kinetic hindrance for this transformation.

Experimental Section

Preparation of the ionic liquid (IL): 1,3-Dibutyl-2-methylimidazolium bis(trifluoromethyl-sulfonyl) azanide ([DBMIM][TFSI], also referred to as 1,3-dibutyl-2-methylimidazolium bis (trifluormethylsulfonyl)imide) was prepared in two-steps comprising the synthesis of 1,3-dibutyl-2-methylimidazolium bromide by reaction of 1-butyl-2-methylimidazole with butyl bromide and a subsequent anion exchange with Li[TFSI]. After synthesis, the vacuum-dried [DBMIM][TFSI] was stored in an argon glovebox over molecular sieve (3 Å, Merck). Details on the preparation and basic characterization of this IL by routine chemical analysis and NMR (^{1}H, ^{13}C, ^{19}F), on its inertness against $Na_{12}Ge_{17}$, on its thermal stability and on the obtained purity have recently been reported elsewhere.[38]

Preparation of $Na_{12}Ge_{17}$: $Na_{12}Ge_{17}$[42] was obtained in batches of about 2 g by reacting a stoichiometric mixture of the elements (Na - Chempur, 99.9%; Ge – Alfa Aesar, 99.9999%, powdered) in a welded Ta ampoule in an argon glovebox at 1100 °C by using an induction furnace (2 min), and allowing the ampoule to cool down within some minutes. The obtained dark-gray ingot consisted solely of the air- and moisture sensitive $Na_{12}Ge_{17}$ according to XRPD characterization as reported for the material before.[38]

Preparation of $Na_{24-\delta}Ge_{136}$, step I: Redox reaction of $Na_{12}Ge_{17}$: $Na_{12}Ge_{17}$ was reacted with benzophenone in the IL [DBMIM][TFSI] by using dry Duran glass equipment in an argon-filled glovebox.[38] 11 ml (12 g, 25.3 mmol) of the IL and 570 mg (3.1 mmol) of dried benzophenone were heated to 70 °C, and 400 mg (0.27 mmol) of finely powdered $Na_{12}Ge_{17}$ were added. The reaction mixture was stirred at constant temperature, optimally for 3d. Subsequently, the solid was allowed to settle, the IL phase was removed by a pipette, and the solid remainder was washed repeatedly with dry toluene (Sigma-Aldrich, anhydrous, 99.8%), typically 10 times 10 ml, under argon atmosphere to dissolve and remove adhesive residuals of the liquid reaction medium and co-products of the reaction. The obtained solid was dried in vacuum, yielding the widely X-ray-amorphous product **I**, which was stored in an argon-filled glovebox.

Preparation of $Na_{24-\delta}Ge_{136}$, step II: Thermal treatment: Product **I** was subjected to a thermal treatment under argon atmosphere (1 bar). Samples of about 130 mg were annealed in an open Duran glass crucible, which was place in a calibrated vertical tube furnace by using a Duran glass tube. The annealing conditions were varied in the range of $320\,^{\circ}C \le T \le 350\,^{\circ}C$ and $4\,h \le t \le 66\,h$. At optimal conditions ($T = 340\,^{\circ}C$, $t = 18\,h$), this preparation step resulted in product **II** containing the crystalline clathrate phase $Na_{24-\delta}Ge_{136}$ ($\delta \approx 2$) with a maximum concentration of about 40 mass-%.

Chemical analysis: To determine the content of Na and Ge, specimens of products **I** and **II** were dissolved in aqueous HNO_3/HF by using a microwave assisted procedure (ETHOS plus 2, MLS) in closed PTFE vessels, and inductively coupled plasma-optical emission spectrometry (ICP-OES, VISTA RL, Varian, matrix-adapted standard) was performed. For the analysis of C, N, O, and H, specimens of about 5 mg were filled into tin capsules. Carrier-gas hot extraction was performed, and the evolving CO/CO_2, H_2O or N_2 were detected by IR spectrometry.[35]

X-ray powder diffraction (XRPD) analysis: XRPD patterns were recorded on a Guinier camera (Huber G670, image plate detector, Cu $K\alpha_1$ radiation, $\lambda = 1.540598$ Å, Ge(111) monochromator, $5 \le 2\theta \le 100°$, $\Delta 2\theta = 0.005°$). The specimens were prepared in an argon glovebox. The finely ground powders were fixed on the sample holder between two polyimide foils (7.5 μm, Kapton, Chemplex), using a thin film of vacuum grease (Lithelen, Leybold) as an adhesive. Rietveld refinement was performed by using the Jana2006 software.[43] It included, besides the structural parameters, the scale factor, a background fit by a Legendre polynomial function, the profile fit of the clathrate phase by a 4-parameter Pseudo-Voigt function, the profile fit for α-Ge by a 5 parameter Pseudo-Voigt function, the lattice parameters of both phases, the sample displacement, the reflection asymmetry due to beam divergence, and the volume fractions.[43] In order to estimate the fraction of not detected phases in the investigated samples, the internal standard LaB_6 (NIST, SRM 660a, $a = 4.1569162(97)$ Å) was admixed with a defined mass-fraction to the XRPD specimens, and the relative mass fractions of the crystalline phases were determined by Rietveld refinement, which accordingly included also a 5-parameter Pseudo-Voigt function for the profile of LaB_6. The lattice

parameter of the internal standard material was not refined and kept constant. By referring the determined relative to the expected absolute mass fraction of the internal standard in the specimen, the mass fraction of the sample components not contributing to Bragg intensities was finally estimated.[21] A model-independent calculation of the unit cell parameter of the clathrate phase and α-Ge was performed with the WinCSD program package[56] by applying a least-squares technique on reflection positions individually determined by pattern deconvolution and corrected with the internal LaB_6 standard. To trace the aging of $Na_{24-\delta}Ge_{136}$ in air, the same powder specimen was repeatedly remeasured after various times of storage.

Scanning electron microscopy (SEM) and energy dispersive X-ray spectroscopy (EDXS): Investigations were performed on a SEM Philips XL30 equipped with LaB_6-cathode and detectors for backscattered and secondary electrons as well as a silicon drift detector for EDXS. Powder specimens were fixed on a conductive carbon foil mounted on an aluminum support.

^{23}Na solid state nuclear magnetic resonance spectroscopy (NMR): The ^{23}Na spectrum of powder specimens of product **II** and of $Na_{12}Ge_{17}$ as a reference material were obtained in static mode and at magic angle spinning conditions (20 kHz), by using a Bruker Avance 500 spectrometer ($B_0 = 11.74$ T) equipped with a standard Bruker MAS probe for ZrO_2 rotors of 2.5 mm diameter. The rotors were filled in an argon glovebox and tightly closed. The spectra were obtained from the Hahn spin echo after a 90°-pulse (1.9 μs) and a 180° pulse (3.8 μs) with the inter-pulse delay of 60 μs, and a recovery time of 500 ms for spectrum accumulation. NaCl solution in water with the frequency of 132.293 MHz served as an external reference, which was measured before data collection for the powder specimens. Product **II** was investigated within 7 days after preparation. Measurements in static mode were performed immediately after preparation, the investigations in magic-angle spinning (MAS) mode were performed subsequently. After this procedure, the sample was recovered, and a specimen thereof was investigated by XRPD, 9 days after preparation of the original material. The lattice parameter of the $Na_{24-\delta}Ge_{136}$ phase had decreased within the expected frame to $a = 15.400(1)$ Å. Also, the reflection broadening was observed, but a second clathrate phase was not yet assignable (Figure S4). The relative mass fraction of clathrate and α-Ge was found unchanged in comparison to the original product **II** material (Table 2), although the total fraction of X-ray amorphous contributions in the investigated specimen was found somewhat larger in the range of 25 mass-%. Still, such a value may be regarded as expectable based on the above characterization of product **II**. A slight temperature increase often occurring on sample spinning in the NMR measurement might, however, also have influenced the changes of product **II**.

Magnetic susceptibility: Magnetic properties in the temperature range $1.8\ K \le T \le 350$ K were measured on a powder specimen of product **II** ($m = 45$ mg, about 4 weeks after preparation and storage in an argon glovebox) contained in a silica tube, by using a SQUID magnetometer (MPMS XL-7, Quantum Design) at external fields between 2 mT and 7 T. The raw data obtained for the magnetic susceptibility were corrected for the diamagnetic contribution of the silica tube, which had been determined beforehand. To account for small ferromagnetic impurities in the range of few ppm (calculated for pure iron), which probably originate from steel tools applied during sample preparation, datasets measured at 3.5 T and 7 T were used to perform an extrapolation to infinite external field by the Honda-Owen method.[57]

Combined differential thermal analysis-thermogravimetry (DTA-TG): The investigations were performed on specimens of about 25 mg starting mass contained in Ta-crucibles with a perforated lid by using an STA 449C Jupiter thermo-microbalance (Netzsch) equipped with a PtRh/Pt thermocouple. The device was entirely housed in an argon-filled glovebox, so that inert conditions were ensured for the whole process of specimen preparation and loading. Flowing gas conditions ($\dot{V} = 100$ ml/min) were realized by using argon with a basic purity of 99.999 volume-%, which was additionally dried and oxygen post-purified by a High Capacity Oxygen/Moisture Trap (Trigon Technologies). The measurements were performed at a constant heating rate of 10 K/min and, in particular cases, at constant temperature after an initial heating ramp. The specimen mass was corrected for buoyancy according to the temperature and time dependent measurement conditions.

Acknowledgements

Funding by Deutsche Forschungsgemeinschaft within the Priority Program SPP1708 is gratefully acknowledged. We thank H. Borrmann, Yu. Prots, and S. Hückmann for the recording of XRPD data, U. Schmidt, A. Völzke, and G. Auffermann for chemical analyses, S. Scharsach for DTA-TG measurements, as well as U. Burkhardt and P. Scheppan for SEM/EDXS experiments. B.B. acknowledges financial support by the Volkswagen-Stiftung. Open access funding enabled and organized by Projekt DEAL.

Conflict of Interest

The authors declare no conflict of interest.

Keywords: intermetallic clathrates · ionic liquids · metastable compounds · redox chemistry · Zintl phases

[1] J. S. Kasper, P. Hagenmuller, M. Pouchard, C. Cros, *Science* **1965**, *150*, 1713–1714.
[2] C. Cros, M. Pouchard, P. Hagenmuller, *J. Solid State Chem.* **1970**, *2*, 570–581.
[3] J. Gallmeier, H. Schäfer, A. Weiss, *Z. Naturforsch.* **1969**, *24b*, 665–667.
[4] C. Cros, M. Pouchard, *C. R. Chim.* **2009**, *12*, 1014–1056.
[5] A. V. Shevelkov, K. Kovnir, *Struct. Bonding (Berlin)* **2011**, *139*, 97–142.
[6] M. A. Kirsanova, A. V. Shevelkov, *Z. Kristallogr.* **2013**, *228*, 215–227.
[7] G. S. Nolas, *The Physics and Chemistry of Inorganic Clathrates*, Springer, Dordrecht, **2014**.
[8] L. Zhu, G. M. Borstad, H. Liu, P. A. Guńka, M. Guerette, J.-A. Dolyniuk, Y. Meng, E. Greenberg, V. B. Prakapenka, B. L. Chaloux, A. Epshteyn, R. E. Cohen, T. A. Strobel, *Sci. Adv.* **2020**, *6*, eaay8361.
[9] J. Gryko, P. F. McMillan, R. F. Marzke, G. K. Ramachandran, D. Patton, S. K. Deb, O. F. Sankey, *Phys. Rev. B* **2000**, *62*, R7707-R7710.
[10] A. Ammar, C. Cros, M. Pouchard, N. Jaussaud, J.-M. Bassat, G. Villeneuve, M. Duttine, M. Ménétrier, E. Reny, *Solid State Sci.* **2004**, *6*, 393–400.
[11] A. M. Guloy, R. Ramlau, Z. Tang, W. Schnelle, M. Baitinger, Yu. Grin, *Nature* **2006**, *443*, 320–323.
[12] D. Y. Kim, S. Stefanoski, O. O. Kurakevych, T. A. Strobel, *Nat. Mater.* **2015**, *14*, 169–173.
[13] a) S. Yamanaka, E. Enishi, H. Fukuoka, M. Yasukawa, *Inorg. Chem.* **2000**, *39*, 56–58; b) J.-M. Hübner, Yu. Prots, W. Schnelle, M. Bobnar, M. König, M. Baitinger, P. Simon, W. Carrillo-Cabrera, A. Ormeci, E. Svanidze, Yu. Grin, U. Schwarz, *Chem. Eur. J.* **2020**, *26*, 830–838; c) O. O. Kurakevych, T. A. Strobel, D. Y. Kim, T Muramatsu, V. V. Struzhkin, *Cryst. Growth Des.* **2013**, *131*, 303–307; d) A. Wosylus, I. Veremchuk, W. Schnelle, M. Baitinger, U. Schwarz, Yu. Grin, *Chem. Eur. J.* **2009**, *15*, 5901–5903; e) I. Veremchuk, A. Wosylus, B. Böhme, M. Baitinger, H. Borrmann, Yu. Prots, U. Burkhardt, U. Schwarz, Yu. Grin, *Z. Anorg. Allg. Chem.* **2011**, *637*,

1281–1286; f) S. Yamanaka, M. Komatsu, M. Tanaka, H. Sawa, K. Inumaru, *J. Am. Chem. Soc.* **2014**, *136*, 7717–7725; g) J.-M. Hübner, W. Carrillo-Cabrera, Yu. Prots, M. Bobnar, U. Schwarz, Yu. Grin, *Angew. Chem. Int. Ed.* **2019**, *58*, 12914–12918; *Angew. Chem.* **2019**, *131*, 13046–13050.
[14] E. Hohmann, *Z. Anorg. Chem.* **1948**, *257*, 113–126.
[15] H. Horie, T. Kikudome, K. Teramura, S. Yamanaka, *J. Solid State Chem.* **2009**, *182*, 129–135.
[16] a) S. Stefanoski, C. D. Malliakas, M. G. Kanatzidis, G. S. Nolas, *Inorg. Chem.* **2012**, *51*, 8686–8692; b) S. Stefanoski, M. Beekman, W. Wong-Ng, P. Zavalij, G. S. Nolas, *Chem. Mater.* **2011**, *23*, 1491–1495.
[17] A. D. Martinez, L. Krishna, L. L. Baranowski, M. T. Lusk, E. S. Toberer, A. C. Tamboli, *IEEE J. Photovolt.* **2013**, *3*, 1305–1310.
[18] P. F. McMillan, J. Gryko, C. Bull, R. Arledge, A. J. Kenyon, B. A. Cressey, *J. Solid State Chem.* **2005**, *178*, 937–949.
[19] B. Böhme, S. Hoffmann, M. Baitinger, Yu. Grin, *Z. Naturforsch.* **2011**, *66b*, 230–238.
[20] a) B. Böhme, A. Guloy, Z. Tang, W. Schnelle, U. Burkhardt, M. Baitinger, Yu. Grin, *J. Am. Chem. Soc.* **2007**, *129*, 5348–5349; b) Y. Liang, B. Böhme, M. Reibold, W. Schnelle, U. Schwarz, M. Baitinger, H. Lichte, Yu. Grin, *Inorg. Chem.* **2011**, *50*, 4523–4528; c) B. Böhme, M. Bobnar, A. Ormeci, S. Peters, W. Schnelle, M. Baitinger, Yu. Grin, *Z. Kristallogr. Cryst. Mater.* **2017**, *232*, 223–233; d) M. C. Blosser, G. S. Nolas, *Mater. Lett.* **2013**, *99*, 161–163; e) A. M. Guloy, Z. Tang, R. Ramlau, B. Böhme, M. Baitinger, Yu. Grin, *Eur. J. Inorg. Chem.* **2009**, 2455–2458.
[21] B. Böhme, *Inorg. Chem.* **2020**, *59*, 11920–11924.
[22] A. Dopilka, A. Childs, S. Bobev, C. K. Chan, *J. Electrochem. Soc.* **2021**, *168*, 020516.
[23] M. Beekman, M. Baitinger, H. Borrmann, W. Schnelle, K. Meier, G. S. Nolas, Yu. Grin, *J. Am. Chem. Soc.* **2009**, *131*, 9642–9643.
[24] a) A. Grüttner, R. Nesper, H. G. von Schnering, *Angew. Chem. Int. Ed. Engl.* **1982**, *21*, 912–913; *Angew. Chem.* **1982**, *94*, 933; b) H. G. von Schnering, M. Schwarz, R. Nesper, *J. Less-Common Met.* **1988**, *137*, 297–310; c) Z. Tang, A. P. Litvinchuk, M. Gooch, A. M. Guloy, *J. Am. Chem. Soc.* **2018**, *140*, 6785–6788; d) F. Kiefer, V. Hlukhyy, A. J. Karttunen, T. F. Fässler, C. Gold, E.-W. Scheidt, W. Scherer, J. Nylén, U. Häussermann, *J. Mater. Chem.* **2010**, *20*, 1780–1786; e) F. Kiefer, A. J. Karttunen, M. Döblinger, T. F. Fässler, *Chem. Mater.* **2011**, *23*, 4578–4586; f) L. M. Scherf, J. Hattendorff, I. Buchberger, S. Geier, H. A. Gasteiger, T. F. Fässler, *J. Mater. Chem. A* **2017**, *5*, 11179–11187.
[25] a) J. Dong, O. F. Sankey, *J. Phys. Condens. Matter* **1999**, *11*, 6129–6145; b) K. Moriguchi, S. Munetoh, A. Shintani, *Phys. Rev. B* **2000**, *62*, 7138–7143; c) D. Daisenberger, P. F. McMillan, M. Wilson, *Phys. Rev. B* **2010**, *82*, 214101; D. Connétable, *Phys. Rev. B* **2010**, *82*, 075209.
[26] a) G. S. Armatas, M. G. Kanatzidis, *Nature* **2006**, *441*, 1122–1125; b) D. Sun, A. E. Riley, A. J. Cadby, E. K. Richman, S. D. Korlann, S. H. Tolbert, *Nature* **2006**, *441*, 1126–1130; c) G. S. Armatas, M. G. Kanatzidis, *Science* **2006**, *313*, 817–820.
[27] D. Neiner, H. W. Chiu, S. M. Kauzlarich, *J. Am. Chem. Soc.* **2006**, *128*, 11016–11017.
[28] M. Zeilinger, L.-A. Jantke, L. M. Scherf, F. J. Kiefer, G. Neubüser, L. Kienle, A. J. Karttunen, S. Konar, U. Häussermann, T. F. Fässler, *Chem. Mater.* **2014**, *26*, 6603–6612.
[29] P. Simon, X.-J. Feng, M. Bobnar, P. Höhn, U. Schwarz, W. Carrillo-Cabrera, M. Baitinger, Yu. Grin, *ACS Nano* **2017**, *11*, 1455–1465.
[30] P. Hagenmuller, R. Naslain, M. Pouchard, C. Cros, *Spec. Publ. Chem. Soc.* **1967**, *22*, 207–221.
[31] C. Cros, M. Pouchard, P. Hagenmuller, *Bull. Soc. Chim. Fr.* **1971**, *2*, 379–386.
[32] a) M. Beekman, J. A. Kaduk, Q. Huang, W. Wong-Ng, Z. Yang, D. Wang, G. S. Nolas, *Chem. Commun.* **2007**, 837–839; b) S. Stefanoski, G. J. Finkelstein, M. D. Ward, T. Zeng, K. Wei, E. S. Bullock, C. M. Beavers, H. Liu, G. S. Nolas, T. A. Strobel, *Inorg. Chem.* **2018**, *57*, 2002–2012.
[33] M. Beekman, J. Gryko, H. F. Rubin, J. A. Kaduk, W. Wong-Ng, G. S. Nolas, *ICT 2005. 24th International Conference on Thermoelectrics*, 2005, IEEE, New York, **2005**, pp. 219–222.
[34] T. Kume, T. Ban, F. Ohashi, H. S. Jha, T. Sugiyama, T. Ogura, S. Sasakia, S. Nonomura, *CrystEngComm* **2016**, *18*, 5630–5638.
[35] B. Böhme, M. Reibold, G. Auffermann, H. Lichte, M. Baitinger, Yu. Grin, *Z. Kristallogr.* **2014**, *229*, 677–686.
[36] B. Böhme, *Neue Präparationswege für intermetallische Verbindungen*, Ph.D. Dissertation, Technische Universität Dresden, **2010**; Logos, Berlin, **2010**.
[37] C. Cros, J.-C. Benejat, *Bull. Soc. Chim. Fr.* **1972**, *5*, 1739–1743.
[38] X.-J. Feng, S. Lerch, H. Biller, M. Micksch, M. Schmidt, M. Baitinger, T. Strassner, Yu. Grin, B. Böhme, *ChemistryOpen* **2021**, *10*, 205–215.
[39] M. E. Straumanis, E. Z. Aka, *J. Appl. Phys.* **1952**, *23*, 330–334.
[40] D. W. J. Cruickshank, A. Kálman, J. S. Stephens, *Acta Crystallogr. Sect. B* **1978**, *34*, 1333–1334.
[41] E. Halwax, H. Völlenkle, *Monatsh. Chem.* **1985**, *116*, 1367–1376.
[42] W. Carrillo-Cabrera, R. Cardoso Gil, M. Somer, Ö. Persil, H. G. von Schnering, *Z. Anorg. Allg. Chem.* **2003**, *629*, 601–608.
[43] V. Petříček, M. Dušek, L. Palatinus, *Z. Kristallogr.* **2014**, *229*, 345–352.
[44] Ch. Baerlocher, L. B. McCusker, L. Palatinus, *Z. Kristallogr.* **2007**, *222*, 47–53.
[45] G. K. Williamson, W. H. Hall, *Acta Metall.* **1953**, *1*, 22–31.
[46] B. Böhme, K. Wei, M. Bobnar, Yu. Prots, U. Burkhardt, M. Baitinger, G. S. Nolas, Yuri Grin, *Z. Kristallogr.* **2017**, *232*, 543–556.
[47] J.-F. Bérar, P. Lelann, *J. Appl. Crystallogr.* **1991**, *24*, 1–5.
[48] V. K. Pecharsky, P. Y. Zavalij, *Fundamentals of Powder Diffraction and Structural Characterization of Materials*, Second Edition, Springer Science + Business Media, New York, **2009**, pp. 538–539.
[49] A. A. Eliseev, V. A. Efremov, G. M. Kuzmicheva, E. S. Konovalova, V. I. Lazorenko, Y. B. Paderno, S. Y. Khlyustova, *Kristallografiya* **1986**, *31*, 803–805.
[50] S. Bobev, S. C. Sevov, *J. Am. Chem. Soc.* **2001**, *123*, 3389–3390.
[51] a) J. He, D. D. Klug, K. Uehara, K. F. Preston, C. I. Ratcliffe, J. S. Tse, *J. Phys. Chem. B* **2001**, *105*, 3475–3485; b) E. Reny, M. Ménétier, C. Cros, M. Pouchard, J. Sénégas, *C. R. Acad. Sci. Ser. IIc* **1998**, *1*, 129–136.
[52] T. Goebel, A. Ormeci, O. Pecher, F. Haarmann, *Z. Anorg. Allg. Chem.* **2012**, *638*, 1437–1445.
[53] P. W. Selwood, *Magnetochemistry (2nd ed)*. Interscience, New York, **1956**, p. 78.
[54] S. Hudgens, M. Kastner, H. Fritzsche, *Phys. Rev. Lett.* **1974**, *33*, 1552–1555.
[55] N. F. Mott, *J. Solid State Chem.* **1973**, *6*, 348–351.
[56] L. Akselrud, Yu. Grin, *J. Appl. Crystallogr.* **2014**, *47*, 803–805.
[57] K. Honda, *Ann. Phys.* **1910**, *337*, 1027–1063.

Manuscript received: June 11, 2021
Accepted manuscript online: July 16, 2021
Version of record online: August 6, 2021

